

Rossby wave propagation on potential vorticity fronts with finite width

B. J. Harvey^{1,2†}, J. Methven² and M. H. P. Ambaum²

¹National Centre for Atmospheric Science (NCAS)

²Department of Meteorology, University of Reading, Reading, UK

(Received xx; revised xx; accepted xx)

The horizontal gradient of potential vorticity (PV) across the tropopause typically declines with lead time in global numerical weather forecasts and tends towards a steady value dependent on model resolution. This paper examines how spreading the tropopause PV contrast over a broader frontal zone affects the propagation of Rossby waves. The approach taken is to analyse Rossby waves on a PV front of finite width in a simple single-layer model. The dispersion relation for linear Rossby waves on a PV front of infinitesimal width is well known; here an approximate correction is derived for the case of a finite width front, valid in the limit that the front is narrow compared to the zonal wavelength. Broadening the front causes a decrease in both the jet speed and the ability of waves to propagate upstream. The contribution of these changes to Rossby wave phase speeds cancel at leading order. At second order the decrease in jet speed dominates, meaning phase speeds are slower on broader PV fronts. This asymptotic phase speed result is shown to hold for a wide class of single-layer dynamics with a varying range of PV inversion operators. The phase speed dependence on frontal width is verified by numerical simulations and also shown to be robust at finite wave amplitude, and estimates are made for the error in Rossby wave propagation speeds due to the PV gradient error present in numerical weather forecast models.

1. Introduction

Large-scale Rossby waves are ubiquitous features of the extra-tropical atmosphere. They typically reside on, and propagate along, the region of large isentropic potential vorticity (PV) gradient at the tropopause. The region of large PV gradient is narrow, in the sense that its width is much smaller than the typical wavelengths of Rossby waves, and as such the jet stream itself meanders latitudinally. A simple model for this PV front is obtained in the limit of a single PV step separating two regions of uniform PV, representing the tropopause as a discontinuity between high PV stratospheric air on the poleward side and low PV tropospheric air on the equatorward side (e.g. Verkley 1994; Swanson *et al.* 1997). The dynamics then reduce to an evolution equation for the lateral displacement of this PV step which can be solved via contour dynamics techniques (Zabusky *et al.* 1979; Pullin 1992).

In reality, however, the width of the region of strong isentropic gradient of PV at the tropopause is finite. Furthermore, the isentropic gradient of PV at the tropopause is found to be systematically too smooth in current global numerical weather prediction (NWP) models, with the gradient typically exhibiting a reduction of around 20% from its initial value over the first three days of a forecast (Gray *et al.* 2014). It is therefore important to understand how the behaviour of Rossby waves on a PV front with small but finite

† Email address for correspondence: b.j.harvey@reading.ac.uk

width differs to those on an infinitely-sharp PV front. Such differences may arise as a modification of the propagation speeds of linear Rossby waves, and also via nonlinear processes such as filamentation and wave breaking which may alter the amplitude of large-scale meanders (see, e.g., Scott *et al.* 2004).

The focus of this paper is the modification of the dispersion relation for Rossby waves on a PV front of infinitesimal width (henceforth a *sharp PV front*) resulting from a smoothing of the PV front. Smoothing the front fundamentally modifies the problem: in the sharp PV front case there exists only a single normal mode, representing north-south meanders of the front, whereas in the smooth case there is an additional continuum of modes representing sheared disturbances within the PV gradient zone. **An additional complication may also arise if critical lines are present on the jet flanks: in the sharp PV front problem the PV gradient is nearly everywhere zero so any critical lines are passive. If the smoothing modifies the basic state PV gradient at the critical line then the linear theory will cease to remain valid. This problem is avoided here by assuming the smoothed basic state PV gradient is at least exponentially small in the smoothing width away from the PV front.**

To explore how the phase speed of waves might be modified on a smooth front, consider the following general form of the dispersion relation of a zonally-propagating wave:

$$c(k) = U_{adv} - c_{int}(k) \quad (1.1)$$

where $c(k)$ is the zonal phase speed of a wave of zonal wavelength k , U_{adv} represents advection by the basic state jet, and $c_{int}(k)$ represents the self-induced, or intrinsic, phase speed of the wave. A westerly extratropical jet is considered for which U_{adv} and $c_{int}(k)$ are both positive. Both U_{adv} and $c_{int}(k)$ depend on the basic state PV profile, and might both be expected to reduce as a sharp PV front is smoothed. The key questions addressed here are: what is the sign of the change in phase speed c resulting from a smoothing, and how does it depend on frontal width? Is a frontal smoothing error of the magnitude present in NWP models expected to have a measurable impact on the propagation of Rossby waves in NWP forecasts?

The propagation of waves on a finite-thickness tropopause has been studied previously using several different approaches. Plougonven & Vanneste (2010) analyse the dynamics of linear waves on a vertical discontinuity in static stability (see Rivest *et al.* 1992) in which the meridional PV gradient is independent of latitude. This represents a broad baroclinic zone with no meridional jet structure. Smoothing this basic state results in a continuous transition from low to high stratification across the tropopause, and the study shows that this acts to *increase* the Rossby wave phase speeds. In the notation of (1.1) the smoother vertical PV profile reduces the ability of waves to propagate upstream (c_{int}) without directly modifying advection by the jet (U_{adv}).

In contrast, the study of Jukes (1998*a,b*) explores the growth rates of baroclinic disturbances in a setup similar to the Eady model: a uniform static stability, uniform PV atmosphere is considered, bounded by rigid horizontal boundaries at the ground and tropopause. Unlike the Eady model, the meridional temperature gradient at the boundaries is confined into a **meridionally-narrow** baroclinic zone, representing the tropopause and temperature gradient at the ground. The associated jet stream is localised in latitude. In this case, smoothing the basic state acts to reduce the jet maximum but it is shown that the growth rates of the baroclinically-growing normal modes are relatively insensitive to the smoothing. Implicit in his equations (e.g. (43a) in Jukes (1998*a*)) it can be seen that the smoothing also acts to *reduce* the phase speeds of the edge waves. This is a result of the smoothing reducing both U_{adv} and $c_{int}(k)$ in (1.1), with the reduction in U_{adv} dominating.

There is clearly a question of which setup is more appropriate, the broad baroclinic zone of Plougonven & Vanneste (2010) or the narrow baroclinic zone of Jukes (1998*a,b*). The present paper follows the approach of Jukes by analysing a model with a narrow PV gradient zone, and an associated jet stream that is localised in latitude. The setup is simplified as much as possible by considering a single-layer model and focusing attention solely on the propagation of Rossby waves. In addition, since the most appropriate 2-d representation of the full 3-d atmosphere is not known precisely, and a number of different 2-d simplified models are often used, the robustness of the asymptotic result for phase speed modification is explored by considering a general family of single-layer PV inversion operators and smoothing kernels.

The analysis begins with a single-layer model with a step function basic state PV profile (described in section 2). A smooth PV front is then generated with finite width r_0 via convolution with a smoothing kernel. The approximate dispersion relation for waves propagating on this smooth basic state, valid for $kr_0 \ll 1$, is derived in section 3. The analysis assumes small wave slope, such that $k\eta \ll 1$ where η represents the size of lateral displacements. Initially the simplest relevant fluid dynamical model is considered, the quasi-geostrophic shallow water (QGSW) equations. In section 4 the results are generalised to a class of similar models with only modest constraints on the PV inversion operator. Implications for errors in operational NWP models are discussed in section 5.1 and some finite-amplitude numerical simulations are presented in section 5.2 to test the robustness of the results at finite wave amplitude (where $k\eta_0 \sim 1$ but $kr_0 \ll 1$). Section 6 presents the key conclusions.

2. Linear waves on a sharp potential vorticity front

The QGSW model (see, e.g., Vallis 2006) represents the large-scale dynamics of a single-layer fluid at small Rossby number. It is commonly used as a model of large-scale atmospheric motions as it incorporates the effects of both rotation and stratification in a simple fashion. The quasi-geostrophic PV, q , is related to the geostrophic streamfunction ψ via

$$q = f + \nabla^2 \psi - \frac{\psi}{L_R^2}, \quad (2.1)$$

where f is the Coriolis parameter, assumed constant, and the Rossby radius of deformation is given by $L_R = \sqrt{gH}/f$ where g is the acceleration due to gravity and H the average layer depth. The horizontal wind is related to the streamfunction via $(u, v) = (-\psi_y, \psi_x)$ where $\mathbf{x} = (x, y)$ are the zonal and meridional coordinates respectively. The dynamics are governed by the Lagrangian conservation of PV following the geostrophic flow:

$$\frac{Dq}{Dt} = 0. \quad (2.2)$$

The QGSW dispersion relation for linear Rossby waves on a sharp PV front is well known (e.g. Swanson *et al.* 1997; Esler 2004; Zhu & Nakamura 2010). Here a brief derivation is provided which highlights, for later reference, the presence of a continuous spectrum of passive singular modes in addition to the familiar discrete meandering mode. Whilst passive for a sharp PV front, the continuous spectrum is important for the finite-width front examined below. The extension to the case of multiple sharp PV steps is then summarised in section 2.1.

The basic state is given by a step-function in PV located at $y = 0$:

$$Q(y) = f + \frac{\Delta}{2} \text{sgn}(y) \quad (2.3)$$

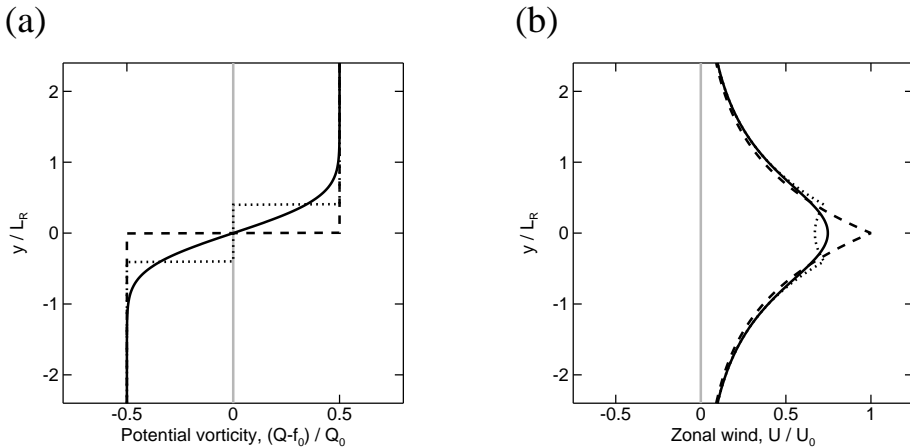


FIGURE 1. Example basic state PV profiles (a) and zonal wind profiles (b) for the single sharp front of (2.3)-(2.4) (dashed lines), the double sharp front of (2.15) (dotted lines), and the smooth front of (3.3)-(3.4) with the Gaussian smoothing kernel (3.33) (solid lines). PV values are scaled by Δ and wind values are scaled by $\Delta L_R/2$. The double sharp front and the smooth front are shown with width $r_0 = 0.4L_R$.

where Δ is the magnitude of the PV jump across the front. The corresponding zonal wind profile is obtained by solving (2.1) for $q = Q(y)$ to obtain

$$u = U(y) = \frac{\Delta L_R}{2} e^{-|y|/L_R}. \quad (2.4)$$

The profiles of $Q(y)$ and $U(y)$ are illustrated by the dashed lines in Figures 1a and 1b respectively.

Considering a perturbation to the basic state, equation (2.2) implies that the PV front is a material contour. Away from the front the PV gradient vanishes, however for generality consider a continuum of passive tracer contours which are advected by the flow but have zero PV contrast: for each $y = \tilde{y}$ of the basic state write the position of the perturbed contour as $y = \tilde{y} + \eta(x, \tilde{y}, t)$, where $y = \eta(x, 0, t)$ is the PV contour. Material advection of these contours implies the kinematic relation

$$\left(\frac{\partial}{\partial t} + u \frac{\partial}{\partial x} \right) \eta(x, y, t) = v \quad (2.5)$$

where u and v are evaluated at $(x, y + \eta(x, y, t), t)$. The dispersion relation is obtained by linearising (2.5) around the basic state (2.3)-(2.4). This is achieved by writing $q = Q + q'$, $u = U + u'$ and $v = v'$ and neglecting terms that are nonlinear in primed quantities, and evaluating all terms at (x, y, t) . In addition, the PV inversion can be calculated by approximating q' as a line distribution along $y = 0$:

$$q' \approx -\eta \Delta \delta(y). \quad (2.6)$$

For a normal mode disturbance of the form $\eta(x, y, t) = \hat{\eta}(y) e^{ik(x-ct)}$, with the small amplitude condition requiring $|k\hat{\eta}| \ll 1$, the streamfunction induced by (2.6) is:

$$\psi' = \phi(y; k) \hat{\eta}(0) e^{ik(x-ct)}, \quad (2.7)$$

where

$$\phi(y; k) = \frac{\Delta L_R}{2\kappa} e^{-\kappa|y|/L_R} \quad (2.8)$$

represents the meridional structure of the perturbation streamfunction for a wavenumber k disturbance, and the *effective wavenumber* is given by $\kappa^2 = 1 + k^2 L_R^2$. In the following, the argument k of ϕ is omitted when the meaning is clear.

After linearisation, (2.5) becomes

$$(U(y) - c) \hat{\eta}(y) = \phi(y) \hat{\eta}(0). \quad (2.9)$$

This equation admits two types of the solution, a discrete mode representing meridional meanders of the PV contour:

$$\hat{\eta}(y) = \hat{\eta}(0) \frac{\phi(y)}{U(y) - c} \quad \text{with} \quad c = U(0) - \phi(0) = \frac{\Delta L_R}{2} \left(1 - \frac{1}{\kappa}\right), \quad (2.10)$$

and a continuous spectrum of singular modes:

$$\hat{\eta}(y) \propto \delta(y - y_0) \quad \text{with} \quad c = U(y_0) \quad \text{for any } y_0 \neq 0. \quad (2.11)$$

The discrete mode (2.10) propagates zonally with speed equal to the sum of advection by the maximum of the basic state jet and an upstream propagation of the Rossby wave proportional to $1/\kappa$. The corresponding group speed:

$$c_g \equiv \frac{\partial}{\partial k}(kc) = \frac{\Delta L_R}{2} \left(1 - \frac{1}{\kappa^3}\right), \quad (2.12)$$

is also slower than the jet maximum for all wavenumbers. The structure of the discrete mode (2.10) is singular where $U(y) = c$, that is at

$$|y| = y_c = L_R \log \left(\frac{\kappa}{\kappa - 1} \right), \quad (2.13)$$

identified with a critical line on each flank of the jet. However, these critical lines are passive since the PV gradient vanishes at all $y \neq 0$ so no PV mixing occurs. Similarly, the continuous spectrum of singular modes (2.11) represent meridional displacements of the passive tracer contours which are localised away from the PV front and as such do not induce any flow. Each mode is localised to a particular value of y and is simply advected by the basic state wind there. Clearly neither the critical lines nor the continuous spectrum play a dynamical role in the sharp PV front problem.

The dispersion relation (2.10) for the discrete mode is qualitatively similar to that of Rossby waves on a uniform PV gradient. For instance, the dispersion relation of linear waves **with zero latitudinal wavenumber** on a uniform wind basic state given by $Q = f + \hat{\beta}y$ and $U = \hat{\beta}L_R^2$, is

$$c = \hat{\beta}L_R^2 \left(1 - \frac{1}{\kappa^2}\right) \quad (2.14)$$

(Vallis 2006) so such waves are advected by the basic state jet and propagate upstream with speed proportional to $1/\kappa^2$. Therefore, short waves on a uniform PV gradient are less able to propagate upstream than their PV front counterparts. Furthermore, the group speed corresponding to (2.14) is easily derived and shown to have a maximum at a finite wavenumber ($\kappa = 4$ in this case) which is faster than the basic state jet speed. It is shown below that these two properties of waves on a uniform PV gradient are recovered when the single sharp PV front is smoothed.

2.1. Potential vorticity fronts composed of multiple sharp PV steps

The procedure for analysing perturbations to a single sharp PV front can be extended to a front composed of multiple parallel PV steps. Instead of the single equation (2.9) for the evolution of a single PV front, one obtains a system of n coupled equations for the evolution of n PV steps. This setup could be used to study the smooth PV front problem by approximating it as a large number of weak PV steps. In the following section the smooth PV front problem is instead considered directly, however the simplest multiple-step case of $n = 2$ is illustrated here since it provides valuable insight into the general problem.

The two steps are taken to be of equal magnitude and spaced a distance $2r_0$ apart:

$$Q_d(y) = \frac{1}{2} (Q(y - r_0) + Q(y + r_0)) \quad (2.15)$$

where $Q(y)$ is the single front basic state PV profile of (2.3) and the subscript d denotes the double front case. By linearity, the corresponding zonal jet profile $U_d(y)$ is likewise equal to the sum of two single front jet profiles and is illustrated in Figure 1b. Due to symmetry, there are now two equal jet maxima located at the locations of the PV fronts, with weaker values in the jet core. Repeating the above analysis for this system one finds two normal mode solutions with phase speeds:

$$c_{\pm} = \frac{1}{2} (U(0) + U(2r_0) - (\phi(0) \pm \phi(2r_0))) \quad (2.16)$$

which represent a meander of the jet (c_+) in which the two contours move in phase with each other, and a **varicose (or jet streak) mode** (c_-) in which the two contours move in anti-phase. Expanding (2.16) for $\epsilon = kr_0 \ll 1$ gives:

$$c_+ = \frac{\Delta L_R}{2} \left(\left(1 - \frac{1}{\kappa} \right) - \frac{\epsilon^2}{\kappa + 1} \right) + O(\epsilon^3) \quad (2.17)$$

$$c_- = \frac{\Delta L_R}{2} \left(1 - \frac{2\epsilon}{\sqrt{\kappa^2 - 1}} \right) + O(\epsilon^3) \quad (2.18)$$

which shows that c_+ reduces to the normal mode solution (2.10) of the single sharp front problem in the limit $\epsilon \rightarrow 0$, whereas c_- collapses onto the jet core speed. Increasing the frontal separation reduces the phase speeds of both modes, but the impact on the meandering mode is quadratic in ϵ due to a leading-order compensation between a reduction in advection by the basic state jet and the ability of the waves to propagate upstream (see equation (1.1)). The phase speed of the varicose mode, in contrast, reduces linearly with ϵ from the jet maximum suggesting that jet streaks are more sensitive to r_0 than the meandering mode. In the next section it is shown that both of these results carry over to the continuous PV gradient case.

3. Linear waves on a potential vorticity front of finite width

In this section an approximate correction to the dispersion relation (2.10) for a smooth PV front with finite width r_0 is derived. The approximation is in terms of the parameter

$$\epsilon = kr_0 \quad (3.1)$$

and is valid in the limit $\epsilon \ll 1$, that is, for smoothing width much smaller than the zonal wavelength. It is also required that $r_0 \ll L_R$.

To generate a smooth basic state, the single sharp front of (2.3) is convolved with a smoothing kernel $w(y; r_0)$ of width r_0 . Such a function should be everywhere positive, so

that the PV gradient remains single-signed. It should also have a domain integral equal to unity, and scale with r_0 in the sense that

$$w(y; r_0) = W(Y)/r_0 \quad (3.2)$$

for some function $W(Y)$, where $Y = y/r_0$. Finally, it is assumed that $w(y; r_0)$ decays exponentially at $|y| \gg r_0$. The argument r_0 of w is omitted when the meaning is clear.

By linearity of the PV inversion operator, the basic state PV and jet are given by:

$$Q_s(y) = \int Q(y')w(y - y') dy' \quad (3.3)$$

$$U_s(y) = \int U(y')w(y - y') dy' \quad (3.4)$$

where $Q(y)$ and $U(y)$ are the single front PV and zonal jet profiles of (2.3) and (2.4) and the subscript s denotes the smooth front case. All integrals shown span the range $(-\infty, \infty)$. Since $Q(y)$ is a step function, the smoothing kernel is proportional to the PV gradient of the smooth basic state:

$$\frac{dQ_s}{dy} = \Delta w(y). \quad (3.5)$$

Therefore the requirement that $w(y)$ decays exponentially at $|y| \gg r_0$ ensures the PV gradient is small away from the front. Example profiles of $Q_s(y)$ and $U_s(y)$ for the Gaussian smoothing kernel of equation (3.33) are illustrated by the solid lines in Figures 1a and 1b respectively.

As for the sharp PV front, the dispersion relation is derived by adding meridional displacements to the basic state PV contours: for each basic state contour position $y = \tilde{y}$, the position of the corresponding perturbed contour is written $y = \tilde{y} + \eta(x, \tilde{y}, t)$. Writing $\eta(x, y, t) = \hat{\eta}(y)e^{ik(x-ct)}$ and linearising the contour advection equation (2.5) for each \tilde{y} gives the following condition for linear waves

$$(U_s(y) - c)\hat{\eta}(y) = \int \phi(y - y')\hat{\eta}(y')w(y') dy', \quad (3.6)$$

where the right hand side is a Green's function expression for the meridional wind. The function $\phi(y)$, defined in (2.8), is the meridional streamfunction structure of a wavenumber k disturbance in the sharp PV front problem.

Equation (3.6) describes the evolution of linear perturbations to the finite-width PV front, analogous to (2.9) for the sharp PV front case. The smoothing results in two modifications to the equation: the advection is by the smooth jet profile $U_s(y)$, and the perturbation streamfunction is given by a convolution over all of the PV contours where the basic state PV gradient $w(y)$ is nonzero. Equation (3.6) is an eigenvalue problem for the meridional structure of the modes $\hat{\eta}(y)$ with corresponding eigenvalues c . Multiplying by $w(y)$ and integrating gives an expression for the eigenvalues in terms of $\hat{\eta}(y)$:

$$c = \frac{\int (U_s(y) - \phi_s(y))\hat{\eta}(y)w(y) dy}{\int \hat{\eta}(y)w(y) dy} \quad (3.7)$$

where, analogous to the definition (3.4) of $U_s(y)$,

$$\phi_s(y) = \int \phi(y - y')w(y') dy'. \quad (3.8)$$

In the remainder of this section it is shown that, as in the sharp PV front problem, equation (3.6) admits two types of solution: a single discrete mode representing large-scale

meanders of the PV front and a continuous spectrum of singular modes which represent sheared disturbances within the frontal zone. **Continuous spectra are a common feature of shear flows in unbounded domains, as identified by Orr (1907), in which often the set of discrete normal modes is incomplete in the sense that it is insufficient to describe arbitrary initial conditions. In the following, the structure and phase speed of the discrete mode are shown to be modified by the smoothing, and their leading-order corrections are derived. The continuous spectrum is shown to be dynamically active, unlike for the sharp PV front case, and details of its structure are discussed.**

3.1. Asymptotic analysis

Equations (3.6) and (3.7) show that the global structure of the modes $\hat{\eta}(y)$ and the phase speeds c are both determined solely by the values of $\hat{\eta}(y)$ in the region where the PV gradient is nonzero, that is where $y = O(r_0)$. As such, an asymptotic analysis of (3.6) is performed in this ‘inner region’, utilising the stretched variable

$$Y = y/r_0. \quad (3.9)$$

Each term in (3.6) is now expanded in terms of ϵ for $Y = O(1)$, allowing coefficients of like-powers to be equated.

First, the Taylor expansion of $U(y)$ is written, for $Y = O(1)$, as

$$U(r_0Y) = U(0) + r_0|Y|U'(0) + \frac{r_0^2}{2}Y^2U''(0) + O(r_0^3), \quad (3.10)$$

where it is understood that the derivatives are evaluated at 0+. Upon substitution into (3.4) the expansion of the smooth basic state jet is found to be

$$U_s(r_0Y) = U(0) + \epsilon f^{(1)}(Y)U'(0) + \frac{\epsilon^2}{2}f^{(2)}(Y)U''(0) + O(\epsilon^3) \quad (3.11)$$

where the following functions have been defined:

$$f^{(n)}(Y) = \frac{L_R^n}{(\kappa^2 - 1)^{n/2}} \int |Y - Y'|^n W(Y') dY' \quad (3.12)$$

and the identity $r_0 = \epsilon L_R / \sqrt{\kappa^2 - 1}$ has been used.

Similarly, the RHS of (3.6) can be expanded in terms of $\phi(0)$ and its derivatives, as presented in Appendix A. Substitution of (3.11) and (A 2) into (3.6) allows a solution to be sought for the inner region as a series expansion in ϵ :

$$\hat{\eta}(y) = \hat{\eta}_0(y) + \epsilon \hat{\eta}_1(y) + \epsilon^2 \hat{\eta}_2(y) + \dots \quad (3.13)$$

$$c = c_0 + \epsilon c_1 + \epsilon^2 c_2 \dots \quad (3.14)$$

Collecting together the $O(1)$ terms of (3.6) gives the following condition relating $\hat{\eta}_0$ and c_0 :

$$(U(0) - c_0)\hat{\eta}_0(y) = \phi(0) \int \hat{\eta}_0(y')w(y') dy'. \quad (3.15)$$

There are two types of solution to (3.15). The first is the single solution

$$\hat{\eta}_0(y) = \text{constant} \quad (3.16)$$

$$c_0 = U(0) - \phi(0), \quad (3.17)$$

and the other is any function satisfying

$$\int \hat{\eta}_0(y)w(y) dy = 0 \quad (3.18)$$

$$c_0 = U(0). \quad (3.19)$$

These two types of solution relate respectively to the discrete mode and the continuous spectrum of singular modes from the sharp PV front problem. **More specifically, it is only that part of the continuous spectrum which is associated with nonzero PV perturbations and as such solutions to (3.18)-(3.19) are the smooth-front extension of the varicose mode from the two-step front problem of section 2.1.** The leading-order corrections to each of these solutions are now considered by examining the $O(\epsilon)$ and $O(\epsilon^2)$ terms of (3.6) in turn, the equations for which are derived in Appendix A.

3.2. The discrete mode

To find the leading-order correction to the normal mode structure and phase speed, the $O(1)$ solution (3.16)-(3.17) is substituted into the $O(\epsilon)$ terms of (3.6), equation (A 5). The result is

$$c_1 \hat{\eta}_0 = \phi(0) \left(\hat{\eta}_1(y) - \int \hat{\eta}_1(y') w(y') dy' \right), \quad (3.20)$$

where the identity $U'(0) = \phi'(0)$ has been used. This identity can be seen to hold for the QGSW system from (2.4) and (2.8); it is shown below to also hold for a general PV inversion operator. Multiplying by $w(y)$ and integrating shows that c_1 must vanish, so the only solution is

$$\hat{\eta}_1(y) = \text{constant} \quad (3.21)$$

$$c_1 = 0. \quad (3.22)$$

Therefore there is no $O(\epsilon)$ correction to the phase speed and an $O(\epsilon^2)$ correction must be sought. There is likewise no $O(\epsilon)$ correction to the structure of the solution in the inner region since the constant $\hat{\eta}_1$ can be absorbed into $\hat{\eta}_0$.

Next consider the $O(\epsilon^2)$ terms of (3.6), equation (A 6). Upon substituting for $\hat{\eta}_0$, $\hat{\eta}_1$, c_0 and c_1 , this reduces to the relation

$$\left(c_2 - \frac{U''(0) - \phi''(0)}{2} f^{(2)}(Y) \right) \hat{\eta}_0 = \phi(0) \left(\hat{\eta}_2(y) - \int \hat{\eta}_2(y') w(y') dy' \right) \quad (3.23)$$

which, again by first multiplying by $w(y)$ and integrating to find c_2 , can be seen to have the solution

$$\hat{\eta}_2(y) = -\frac{U''(0) - \phi''(0)}{2\phi(0)} \left(f^{(2)}(Y) - \int f^{(2)}(Y') W(Y') dY' \right) \hat{\eta}_0 \quad (3.24)$$

$$c_2 = \frac{U''(0) - \phi''(0)}{2} \int f^{(2)}(Y') W(Y') dY', \quad (3.25)$$

where $U''(0) - \phi''(0) = \Delta(1 - \kappa)/2L_R < 0$. Therefore there is an $O(\epsilon^2)$ correction to both the phase speed and the structure of the normal mode in the inner region.

Returning to the full expression for $\hat{\eta}$ of (3.6), an approximate solution can now be found for all y by substituting the $O(\epsilon^2)$ expression for $\hat{\eta}(y)$ in the inner region into the right hand side of (3.6) to find

$$\hat{\eta}(y) = \hat{\eta}_0 \frac{\phi_s(y)}{U_s(y) - c} + O(\epsilon^3). \quad (3.26)$$

Similarly, a convenient form of the phase speed can be recovered from (3.7)

$$c = c_m \equiv \int (U_s(y) - \phi_s(y)) w(y) dy + O(\epsilon^4). \quad (3.27)$$

Note that the error here is $O(\epsilon^4)$, as shown in Appendix B, which is a remarkable result. The quadratic correction of the normal mode structure in the inner region has yielded a cubic correction to the phase speed. It can be shown that $c_m = c_0 + \epsilon^2 c_2 + O(\epsilon^3)$, so (3.7) is equivalent to the series expansion derived above but with an extra order of accuracy. In addition, the form of (3.27) is particularly attractive since it retains explicitly a term associated with advection by the basic state, which is given by the jet profile weighted by the PV gradient, and a term associated with upstream propagation. Both of these terms reduce linearly with ϵ for small ϵ , but their sum reduces quadratically.

As with the sharp front solution (2.10) there is a critical line on each flank of the jet, located at $|y| = y_c$ with $U_s(y_c) = c$, associated with singularities in the structure of the discrete normal mode (3.26). It can be shown that the smoothing does not move the critical line far from the sharp PV case: the correction to y_c from (2.13) is only $O(\epsilon^2)$. Unlike the sharp front problem, the critical line may potentially play an active role in the evolution since the PV gradient does not necessarily vanish at $|y| = y_c$. However, since the PV gradient $w(y)$ is assumed to decay exponentially at large $|y|/r_0$, any mixing of PV at the critical line will not influence the leading-order correction of the wave structure or its phase speed provided $y_c \gg r_0$, which is the case for $\epsilon \ll 1$.

3.2.1. Properties of c_m

A key property of the approximate phase speed c_m of the discrete normal mode is that it reduces quadratically for small ϵ . Here it is shown that in addition c_m decreases monotonically for all ϵ . The expression is then evaluated explicitly for a Gaussian smoothing kernel.

First it is noted that c_m can be written directly in terms of the sharp front functions

$$c_m = \int (U(y) - \phi(y)) x(y) dy \quad (3.28)$$

where $x(y)$ is the self-convolution of the smoothing kernel:

$$x(y) = \int w(y - y') w(y') dy'. \quad (3.29)$$

Substituting for $U(y)$ and $\phi(y)$ and differentiating with respect to r_0 gives

$$c_m = \frac{\Delta L_R}{2} \int \left(e^{-r_0|Y|/L_R} - \frac{e^{-\kappa r_0|Y|/L_R}}{\kappa} \right) X(Y) dY \quad (3.30)$$

where, analogous to the [definition](#) (3.2) of $W(Y)$, $X(Y) = r_0 x(y/r_0)$. Therefore,

$$\frac{dc_m}{dr_0} = -\frac{\Delta}{2} \int |Y| \left(e^{-r_0|Y|/L_R} - e^{-\kappa r_0|Y|/L_R} \right) X(Y) dY \leq 0 \quad (3.31)$$

with the inequality a result of the fact that $\kappa \geq 1$, implying that the term in parentheses is non-negative for all Y and r_0 . Therefore c_m always reduces if the width of smoothing is increased, indicating that the influence of smoothing on the advection term dominates the influence of smoothing on the self-propagation term.

In the limit of large ϵ , it is of note that c_m has the same form as the dispersion relation (2.14) for Rossby waves on a uniform PV gradient. For large ϵ , expanding $X(Y)$ as a Taylor series around $Y = 0$ in (3.30) and integrating gives

$$c_m = \frac{\Delta X(0)}{r_0} L_R^2 \left(1 - \frac{1}{\kappa^2} \right) + O(\epsilon^{-3}), \quad (3.32)$$

which equivalent to (2.14) in the limit $\epsilon \rightarrow \infty$, with corresponding PV gradient given by $\hat{\beta} = \Delta X(0)/r_0$.

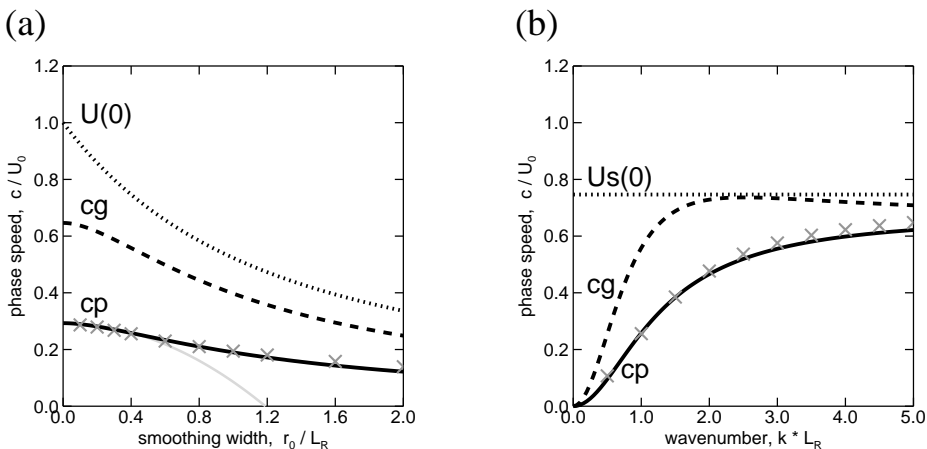


FIGURE 2. The smooth front dispersion relation (3.27) evaluated for the Gaussian smoothing kernel (3.35). Both panels show phase speeds (solid), group speeds (dashed) and the basic state jet maxima (dotted). (a) speeds as a function of r_0 for fixed wavenumber $kL_R = 1$ together with the quadratic approximation (3.25) (grey line). (b) speeds as a function of k for fixed smoothing width $r_0 = 0.4L_R$. Both panels also show the results of finite amplitude numerical simulations ($k\eta_0 = 0.1$, grey symbols) as described in section 5.2. All values are scaled by $U_0 \equiv \Delta L_R/2$.

Finally it is noted that for the Gaussian kernel function,

$$w(y; r_0) = \frac{e^{-y^2/2r_0^2}}{\sqrt{2\pi r_0}}, \quad \text{i.e.,} \quad W(Y) = \frac{e^{-Y^2/2}}{\sqrt{2\pi}}, \quad (3.33)$$

the jet maximum takes the value

$$U_s(0) = \frac{\Delta L_R}{2} E\left(\frac{r_0}{\sqrt{2}L_R}\right), \quad (3.34)$$

where the function $E(x) = e^{x^2}(1 - \text{erf}(x))$ is the scaled complementary error function, equation (3.29) evaluates as $x(y) = w(y/\sqrt{2})/\sqrt{8}$ and the approximate phase speed (3.30) can be evaluated as

$$c_m = \frac{\Delta L_R}{2} \left(E\left(\frac{r_0}{L_R}\right) - \frac{1}{\kappa} E\left(\frac{\kappa r_0}{L_R}\right) \right), \quad (3.35)$$

Figure 2 shows values of (3.35) and the corresponding group speeds for a range of r_0 with fixed k (panel a), and a range of k with fixed r_0 (panel b). Panel a shows that both quantities decrease with the smoothing width r_0 and that their gradients tend to zero at small r_0 ; panel b shows that the group speed has a maximum at intermediate k which is faster than the advecting velocity, qualitatively similar to the dispersion relation (2.14) for Rossby waves on a uniform PV gradient.

3.3. The continuous spectrum of singular modes

Similar to above, the structure of the singular modes are examined further by substituting what is known of the $O(1)$ solution (3.18)-(3.19) into the $O(\epsilon)$ truncation of (3.6), equation (A 5), giving

$$\left(U'(0)f^{(1)}(Y) - c_1 \right) \hat{\eta}_0 = \phi'(0)g^{(1)}(Y; \hat{\eta}_0) + \phi(0) \int \hat{\eta}_1(y')w(y') dy' \quad (3.36)$$

where the function $g^{(1)}(Y; \hat{\eta}_0)$ is defined in (A 3). Multiplying by $w(y)$ and integrating shows that the final term $\int \hat{\eta}(y)w(y) dy$ must vanish (using $U'(0) = \phi'(0)$ again), resulting in extra information about $\hat{\eta}_0(y)$: as well as satisfying (3.18) it must satisfy the new integral eigenvalue equation given by (3.36) with the final term removed. Therefore for the singular modes the $O(1)$ solution is only determined by considering the $O(\epsilon)$ terms.

Assuming no further discrete modes exist satisfying these criteria, it can be anticipated that the leading-order singular mode solution should satisfy (3.36), and its phase speed will take the form $c = c_0 + \epsilon c_1$ with $c_1 = U'(0)f^1(Y; 1)$ for some Y . That is, their phase speeds reduce linearly with ϵ . More generally, from the form of (3.6) it can be expected that singular modes exist with any phase speed in the range $c \in [0, U_s(0)]$. However, those that live outside of the inner region examined here, that is those with $c = U_s(y_0)$ with $w(y_0)$ small, will be passive, like the entire continuous spectrum of the sharp PV front problem. **Those inside the inner region behave as described above: as $\epsilon \rightarrow 0$ the phase speeds of these modes collapse onto the jet core speed of the sharp front problem.**

Combining this result with the previous section, it can be expected that a general initial condition can be projected onto a linear combination of the discrete normal mode and the continuous spectrum of singular modes. The evolution is then determined by each mode propagating independently at its phase speed. Typically in sheared flow problems, the energy contained in singular modes decays with time as they are sheared out (Orr 1907; Farrell 1982; De Vries *et al.* 2009), although transient growth can occur via the Orr mechanism. Therefore at long times the solution will reduce to the projection of the initial condition onto the discrete normal mode. For a linear shear flow the long-time decay of energy in the continuous spectrum scales like t^{-2} (Orr 1907), however in the present case the shear is not linear (there is a stationary point at the jet core for any smooth $w(y)$), and it is expected that the decay will be slower than t^{-2} , although no attempt is made to quantify this here.

4. Generalisation to alternative Green's functions

The previous sections used the QGSW model. In this section it is shown that the expression (3.27) for Rossby wave phase speeds on a smooth PV front is valid for a wide range of inversion operators, and the key property of a quadratic dependence of the phase speed on ϵ requires only a modest condition on the Green's function.

The general setup of a 2-d fluid model resulting from an advected PV field with a linear inversion operator is considered, and the Green's function for the PV inversion operator, denoted $G(x)$, is assumed to (i) be differentiable except for a possible singularity at $x = 0$, and (ii) not grow as fast as x at large x . The expression (2.4) for the jet induced by a single sharp PV front formally generalises to the contour integral formula (Pullin 1992)

$$U(y) = -\Delta \int G\left(\sqrt{x^2 + y^2}\right) dx. \quad (4.1)$$

However, this integral fails to converge if $G(x)$ does not decay sufficiently fast at large x . To ensure convergence for all relevant G , the integral is instead written

$$U(y) = -\Delta \int \left(G\left(\sqrt{x^2 + y^2}\right) - G\left(\sqrt{x^2 + y_0^2}\right) \right) dx \quad (4.2)$$

where y_0 is arbitrary and the second term in the integrand is effectively a constant of integration such that $U(y_0) = 0$. The integral may fail to converge at small x only when $y = 0$ if the singularity in G is not integrable, in the sense that the 1-d integral $\int_0^a G(x) dx$ is finite for any a . In that case the basic state jet has a singularity at the location of

the PV front, as is the case for example in surface QG dynamics (Jukes 1995; Harvey & Ambaum 2010), but is finite at all other y . Similar to (4.2), the expression (2.8) for the meridional structure of the streamfunction perturbation in the single sharp PV front case generalises to

$$\phi(y) = -\Delta \int \left(G(\sqrt{x^2 + y^2}) - G(\sqrt{x^2 + y_0^2}) \right) \cos(kx) dx, \quad (4.3)$$

where the appropriate solution is obtained by taking $y_0 \rightarrow \infty$.

An expression for the dispersion relation for disturbances on a single sharp PV front in this general case is readily obtained by substituting (4.2) and (4.3) into (2.10). Similarly, the expression (3.27) for the approximate phase speed of the discrete normal mode for the smoothed PV front is obtained from substituting (4.2) and (4.3) into (3.28):

$$c_m = -\Delta \int X(Y) (U(r_0 Y) - \phi(r_0 Y)) dY \quad (4.4)$$

where $X(Y)$ is defined below (3.30). The Y integral in (4.4) is a smoothing operation which will not change the dependence on r_0 , therefore the behaviour of c_m at small r_0 is determined by the term in parentheses. To test if this variation is quadratic, one can differentiate the term in parentheses with respect to r_0 and integrate the x -integrals by parts to obtain

$$\frac{d(U(r_0 Y) - \phi(r_0 Y))}{dr_0} = \Delta r_0 \int G(\sqrt{x^2 + r_0^2 Y^2}) \left(k \frac{\sin(kx)}{x} - \frac{1 - \cos(kx)}{x^2} \right) dx. \quad (4.5)$$

Due to the factor r_0 in front of the integral, it is clear that c_m will vary quadratically with r_0 for small r_0 if the integral is finite in the limit $r_0 \rightarrow 0$. At large x the integral will converge if $G(x)$ does not grow as fast as x , as is assumed, and at small x the term in parentheses is finite:

$$k \frac{\sin(kx)}{x} - \frac{1 - \cos(kx)}{x^2} = \frac{k^2}{2} + O(x^2). \quad (4.6)$$

Therefore the integral will converge if the singularity in G is integrable. This condition is equivalent to requiring that $U(0)$ is finite. In conclusion, the expression for the approximate phase speed of the meandering component (4.4) varies quadratically for r_0 for small r_0 for any choice of Green's function provided the jet of the corresponding sharp PV front is not singular.

4.1. Illustration for a family of inversion operators

To illustrate this property, and examine the transition from a regular jet to a singular one, the calculation is performed for the so-called α -turbulence family of Green's functions introduced by Pierrehumbert *et al.* (1994). These inversion operators are defined most simply in spectral space for which

$$\hat{\psi}(|\mathbf{k}|) = -\frac{\hat{q}(|\mathbf{k}|)}{|\mathbf{k}|^\alpha} \quad (4.7)$$

where $\alpha > 0$ is a real number and hats denote 2-d Fourier transforms. Physically-realizable members of the family include 2-d Euler dynamics ($\alpha = 2$) and surface QG dynamics ($\alpha = 1$) (Held *et al.* 1995), which represent the limits of deep and shallow 3-d QGPV anomalies respectively. As such, the horizontal structure of a 3-d PV distribution may be expected to qualitatively satisfy (4.7) with $1 < \alpha < 2$. Iwayama & Watanabe (2010) derive expressions for the corresponding Green's functions and also argue that

$\alpha > 3$ is unphysical, so here the attention is restricted to the range $0 < \alpha < 3$ for which the Green's function of Iwayama & Watanabe (2010) can be written as

$$G(x) = \Psi(\alpha)(|x|^{\alpha-2} - 1) \quad \text{with} \quad \Psi(\alpha) = \frac{-1}{2^\alpha \sin(\pi\alpha/2)\Gamma(\alpha/2)^2}. \quad (4.8)$$

The function $\Psi(\alpha)$ is singular at $\alpha = 2$, but the combination in (4.8) is regular in the limit $\alpha \rightarrow 2$ and reduces to the familiar 2-d Euler Green's function $G(x) = \log(x)/2\pi$ in that case. The Green's function (4.8) is differentiable everywhere except $x = 0$ and it does not grow as fast as x at large x for all $\alpha < 3$. However, the singularity at $x = 0$ is only integrable when $\alpha > 1$. Therefore the approximate phase speed (4.4) of the discrete normal mode is expected to vary quadratically for small r_0 for $\alpha > 1$, but not for $\alpha \leq 1$.

To test this assertion, the integrals (4.2), (4.3) and (4.4) are evaluated explicitly for the α -turbulence model in Appendix C. The following expressions are obtained for the basic state jet and dispersion relation of the single sharp PV front

$$U(y) = U_0 - A(\alpha)|y|^{\alpha-1} \quad \text{with} \quad A(\alpha) = -\frac{\Delta}{2 \cos(\pi\alpha/2)\Gamma(\alpha)} \quad (4.9)$$

$$c = U_0 - \frac{B(\alpha)}{|k|^{\alpha-1}} \quad \text{with} \quad B(\alpha) = \frac{\Delta\Gamma(\alpha-1)}{2^{\alpha-1}\Gamma(\alpha/2)^2} \quad (4.10)$$

where U_0 is a constant. As anticipated, the basic state jet (4.9) is finite everywhere for $\alpha > 1$ but singular at $y = 0$ for $\alpha \leq 1$. For the special case $\alpha = 1$ the function $A(\alpha)$ is singular, but the combination in (4.9) is regular in the limit $\alpha \rightarrow 1$ (with a suitable choice of U_0 , see appendix) resulting in the logarithmic velocity singularity of a surface QG temperature front $U(y) = -(\Delta/\pi) \log|y/y_0|$ (Harvey & Ambaum 2010). In contrast, the phase speeds (4.10) are finite for all $\alpha > 0$, despite the singularity in the basic state wind field when $\alpha \leq 1$. Again $\alpha = 1$ is a special transitional case but as above it is straightforward to recover the well-known relation for surface QG waves on a temperature front $c = (\Delta/\pi) \log|ky_0|$ (Harvey & Ambaum 2010).

The integral (4.4) is also evaluated explicitly in Appendix C, and the leading-order terms in $\epsilon = kr_0$ are shown to take the form

$$c_m(r_0) \approx U_0 - \frac{B(\alpha)}{|k|^{\alpha-1}} + \frac{1}{|k|^{\alpha-1}} \left(\epsilon^{\alpha+1} C_1(\alpha) \int X(Y)Y^{\alpha+1} dY + \epsilon^2 C_2(\alpha) \int X(Y)|Y|^2 dY \right) \quad (4.11)$$

where the functions $C_1(\alpha)$ and $C_2(\alpha)$ are given in Appendix C. The first two terms on the right hand side of (4.11) are the exact result for the linear phase speed on a sharp PV front of (4.10). The final two terms are the two leading-order corrections due to smoothing. For $\alpha > 1$ the C_2 term dominates and $C_2(\alpha) < 0$ meaning that $c_m(r_0)$ decreases quadratically with ϵ . For $\alpha < 1$ the PV inversion operator becomes more local, the jet becomes singular, and the C_1 term dominates resulting in the phase speed varying faster than a quadratic. These properties confirm the result above that c_m is quadratic in ϵ if the singularity in G is integrable.

5. Implications for the error in numerical weather forecast models

5.1. Typical dimensional values

Returning to the dispersion relation for the QGSW model with a Gaussian smoothing kernel (3.35), typical numbers are now used to estimate the potential error in phase speeds resulting from the systematic smoothing of the PV at the tropopause by NWP models. The magnitude of the smoothing error has recently been evaluated for several state-of-

	r_0 [km]	r_0/L_R	$U_s(0)$ [ms ⁻¹]	$c_m(r_0)$ [ms ⁻¹]	$d(kc_m)/dk(r_0)$ [ms ⁻¹]
Sharp PV front	0	0	70.0	20.5	45.3
Typical analysis values	308	0.440	50.9	17.7	38.2
Typical 5-day forecast values	381	0.544	47.6	16.8	36.0

TABLE 1. Typical values for the Gaussian smoothing kernel of the jet maximum $U_s(0)$ from (3.34) and the phase and group speeds from (3.35) with wavenumber $kL_R = 1$. The values of r_0 are taken from Gray *et al.* (2014) and all other parameter values are as described in the text.

the-art weather forecast models by Gray *et al.* (2014). They found that the decrease in the isentropic gradient of PV at the tropopause typically occurs during the first three days of a forecast, during which time the maximum isentropic PV gradient decays by at least 20% from the analysis value to a lower value dependent on model and resolution.

Typical dimensional values for the PV front model relevant to the extratropical tropopause region are given by Swanson *et al.* (1997) and Esler (2004) as $L_R = 700$ km and $\Delta = 2 \times 10^{-4} \text{ s}^{-1}$. These result in a value of $U(0) = \Delta L_R/2 \approx 70 \text{ ms}^{-1}$ for the strength of the jet maximum and the following values for the phase speed of Rossby waves from equation (2.10)

$$c \approx 70 \left(1 - \frac{1}{\kappa} \right) \approx \begin{cases} 0 \text{ ms}^{-1}, & k \rightarrow 0 \\ 20 \text{ ms}^{-1}, & kL_R = 1, \end{cases} \quad (5.1)$$

where $k \rightarrow 0$ is the long wave limit and $kL_R = 1$ is typical of baroclinic waves. It should be noted that this value of jet maximum represents a local wind speed value; nonlinear waves of realistic amplitude considerably reduce the zonal mean wind speed.

A typical isentropic gradient of Ertel PV at the troposphere-stratosphere boundary to the northern side of wintertime ridges in analyses is 1.30 PVU per 100 km, and in 5-day forecasts is 1.05 PVU per 100 km (Gray *et al.* 2014). Taking a typical PV contrast across the tropopause of 4 PVU therefore gives typical widths of the tropopause front on an isentropic surface of $r_0 = 308$ km and $r_0 = 381$ km in analyses and 5-day forecasts respectively. The values of the jet maximum and the phase and group speeds for wavenumber $kL_R = 1$ from these two cases are presented in Table 1, in addition to the values for a sharp PV front ($r_0 = 0$) for reference.

The jet maximum decreases as r_0 increases, with the analysis value 19 ms⁻¹ slower than the sharp PV front value and the 5-day forecast value a further 3 ms⁻¹ slower than the analysis value. The phase speeds are less sensitive to changes in r_0 , with the 5-day forecast value only 1 ms⁻¹ slower than the analysis value, and the change in group speed lies between two with the 5-day forecast value 2 ms⁻¹ slower than the analysis value. The near compensation between the advection and propagation terms in the dispersion relation means that the phase speed correction is smaller than the basic state jet correction. However, a 1 ms⁻¹ error over a period of 5 days would result in a phase error of 430 km. There is a similar first-order cancellation in the group speed, although the variation in group speed with r_0 is over twice as large as the variation in phase speed in this case. This may impact the ability of the forecast models to accurately predict downstream development events which result from the zonal propagation of Rossby wave activity.

5.2. Numerical validation and finite amplitude illustration

A numerical QGSW code has been used to verify the analytic dispersion relation (3.35) for a smooth PV front. The aim is twofold, first to perform a simple verification

of the linear theory in the case of small amplitude disturbances and second to present an illustration of the finite amplitude case.

The code used is based on that used in Harvey & Ambaum (2011): a semi-Lagrangian scheme is used to advect the PV q around a doubly-periodic domain, and inversion is performed in spectral space. The initial condition is specified as the smoothed PV front given by (3.3) with the Gaussian smoothing kernel (3.33) a single wavenumber perturbation of the form:

$$q(x, y) = \frac{\Delta}{2} \operatorname{erf} \left(\frac{y - \eta(x)}{2r_0} \right) \quad \text{with} \quad \eta(x) = \hat{\eta}_0 \cos(kx). \quad (5.2)$$

To diagnose the wave speed the quantity $\overline{(q(t) - q(0))^2}$ is considered, where the overbar denotes the domain average, and the phase speed is calculated from the timing of the first minimum of this quantity.

The symbols in Figure 2 show results from integrations using small amplitude disturbances ($\hat{\eta}_0 = 0.1L_R$). They show that the dispersion relation (3.35) is remarkably accurate in this case. For $kL_R = 1$ (panel a) the accuracy of the numerical result degrades as the smoothing width increases, but the error is within 2.3% of the analytic value when $r_0/L_R < 1$, and within 14.2% when $r_0/L_R < 2$. For fixed $r_0/L_R = 0.4$ (panel b) the accuracy of the numerical result degrades as the wavenumber increases but is within 2.4% of the analytic value when $kL_R < 2$.

The accuracy of the analytic result also varies with the disturbance amplitude $\hat{\eta}_0$ since for larger waveslopes nonlinear terms will become important. Esler (2004) derives a weakly nonlinear theory for waves on a sharp PV front and shows that the phase speed decreases quadratically with the wave amplitude, at small amplitudes, due to a reduction of advection by the basic state. In the smooth PV front case there are also additional complications such as the presence of nonlinear filamentation of PV. In this paper attention is restricted to some simple numerical simulations to provide an illustration of the large amplitude case. The aim is to address the pragmatic question: does the impact of the smoothing on the phase speeds, as presented in Table 1, vary strongly with wave amplitude?

Figures 3a and b show PV snapshots from two integrations with wavenumber $kL_R = 1$ and initial waveslope $k\hat{\eta}_0 = 1$. The two integrations have smoothing widths of $r_0 = 0.440L_R$ and $r_0 = 0.544L_R$, corresponding respectively to the analysis and forecast model estimates from the previous section, and the snapshot time corresponds to approximately 1.3 wave cycles into the integration. Filamentation of PV away from the front is clearly present and, as anticipated, there is more filamentation in the smoother PV front case (panel b). Panel c shows the difference between the two PV fields, with the positions of the zero contours indicating the phase difference between the two cases. The wave on the smoother PV front travels more slowly than the wave on the sharper PV front, and its amplitude decays as a result of meridional divergence of wave activity.

To quantify how the phase speed varies with wave amplitude, integrations have been performed for a range of amplitude values between $k\hat{\eta}_0 = 0.1$ and $k\hat{\eta}_0 = 1.4$ and the phase speed estimated as above. Figure 4 shows that the phase speeds decrease approximately quadratically as the wave amplitude increases, consistent with the theory of Esler (2004). The difference between the two simulations represents the error between propagation speeds in analyses and model forecasts, and this quantity decreases with wave amplitude: at waveslope $k\hat{\eta}_0 = 1$ the correction due to finite r_0 is reduced by 35%. The corresponding dimensional values for the phase speeds, using the typical parameter values discussed above, are $c_m = 15.5 \text{ ms}^{-1}$ and 14.8 ms^{-1} .

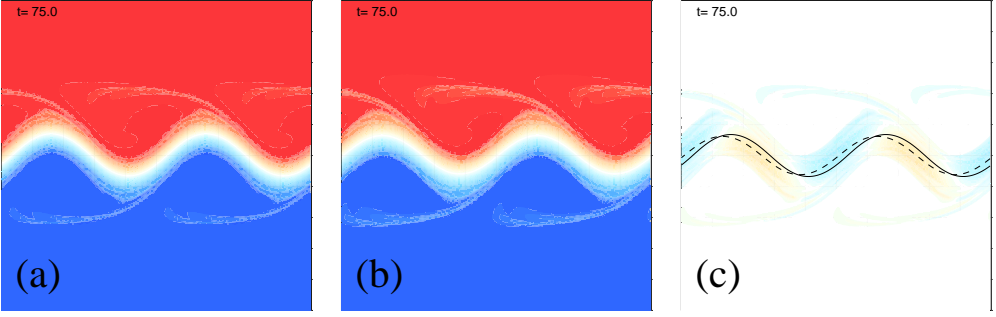


FIGURE 3. PV snapshots at time $t = 75/\Delta$ from QGSW model integrations of the initial condition (5.2). (a) $r_0 = 0.440L_R$ and (b) $r_0 = 0.544L_R$, and (c) the difference (b)-(a). Both integrations have wavenumber $kL_R = 1$ and initial waveslope $k\hat{\eta}_0 = 1$. High and low PV values are indicated by red and blue respectively, and the two contours in panel c are the zero PV contours from panel a (solid) and panel b (dashed) respectively.

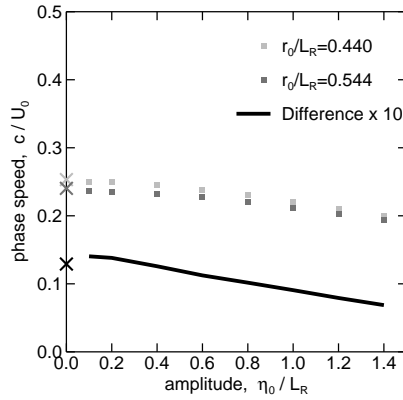


FIGURE 4. Numerically-obtained phase speeds as a function of wave amplitude for smoothing widths $r_0/L_R = 0.440$ (light grey) and $r_0/L_R = 0.544$ (dark grey). The solid line shows the difference in phase speed for the two values of r_0 (multiplied by 10 for ease of viewing). The crosses on the y-axis indicate the results from the linear theory for comparison.

6. Conclusions and Discussion

The dispersion relation for linear Rossby waves on a PV front of infinitesimal width is well known for the quasi-geostrophic shallow water model (QGSW). In this paper a smooth PV front of small but finite width r_0 is considered. It is shown that the single discrete normal mode of the sharp PV front problem, representing north-south meanders of the front, **still exists on a smooth front provided the PV gradient remains negligible at the latitudes of the critical lines. In addition there is a continuous spectrum of singular modes, representing internal structure at the front.** The leading-order correction to the discrete mode structure and phase speed are derived, valid in the limit $\epsilon = kr_0 \ll 0$ where k is zonal wavenumber. In addition, the analysis is generalised to the α -**turbulence** family of single-layer fluid dynamics models. This paper has demonstrated that

- Rossby wave phase speeds are relatively insensitive to the smoothing width r_0 due to a leading-order cancellation between a reduction in advection by the jet and the ability of waves to propagate upstream; and
- at $O(\epsilon^2)$ the reduction in advection dominates, resulting a decrease of phase speeds with r_0 .

Both properties are robust across a wide class of single-layer PV dynamics with varying scale-affect of PV inversion. Therefore, even though the most appropriate single-layer proxy for Rossby wave propagation in the 3-d atmosphere is unknown, the results derived here are likely to hold whatever the precise form assumed.

The result is applied to mid-latitude Rossby waves, which reside on the region of large isentropic PV gradient at the tropopause. In reality the PV front has a finite width, and furthermore, current global numerical weather prediction models are known to evolve towards having a PV front which is too broad. Typical numbers from analyses and forecast models are taken from Gray *et al.* (2014) and used to estimate a typical error in the propagation speeds of Rossby waves in the forecast models. The smoother tropopause in the forecast results in phase speeds that are typically too low by 1 ms^{-1} , which over a 5-day period amounts to a phase error of 400 km, and group speeds that are too low by 2 ms^{-1} . The result is systematic for both phase and group speed and therefore likely to result in systematic large-scale model error in forecasts.

An important caveat to these results is that they are based on linear theory. Typical atmospheric Rossby waves have non-negligible wave slopes, of order 1, which can act to slow their eastward propagation (Esler 2004). **Whilst the theory presented here is only valid for small amplitude disturbances**, it is shown from numerical simulations that at finite amplitude the impact of smoothing on phase speeds is smaller than predicted, but only by around 35% at a realistic waveslope $k\eta = 1$.

Finally, it is noted in the discussion of the finite amplitude illustration that additional processes may be important in that case. In particular, simulations of smoother PV fronts exhibit stronger filamentation of PV away from the front (see figure 3). Such filamentation, which is neglected in the linear theory, **will lead to a sharpening of the jet by erosion**, but may also be expected to result in a reduction in the amplitude of the Rossby wave due to enhanced meridional dispersion of wave activity (see, e.g. Scott *et al.* 2004). This may have two important consequences. First, in addition to quantifying the systematic smoothing of the tropopause PV gradient in NWP models, Gray *et al.* (2014) noted that on average model forecasts tend to under-predict the amplitude of Rossby waves. The average ridge amplitude typically decreases from the analysis value to a smaller, model dependent value over the first five days of a forecast. It is possible that increased filamentation and PV mixing on the jet flanks (a more ‘lossy’ waveguide) could contribute to this bias and this process is, **as explained previously, missing from the analytical treatment presented above**. Second, assuming the reason the tropopause is too smooth in the models is excessive numerical diffusion, the action of the filamentation to enhance the PV gradient will be balanced by larger diffusion fluxes of PV in the jet core. It could be anticipated that these mechanisms combined provide a route whereby small scale diffusion can systematically damp large scale waves. Both of these consequences are currently under investigation.

This work was supported by the Natural Environment Research Council through NCAS-Atmospheric Physics National Capability funding and the DIAMET project [grant NE/I005196/1].

Appendix A. Asymptotic expansion of the evolution equation (3.6)

In order to expand (3.6) in powers of ϵ the Taylor expansion of $\phi(y)$ is written, for $Y = O(1)$, as

$$\phi(r_0 Y) = \phi(0) + r_0 |Y| \phi'(0) + \frac{r_0^2}{2} Y^2 \phi''(0) + O(r_0^3), \quad (\text{A } 1)$$

where it is understood that the derivatives are evaluated at 0+. Upon substitution into the RHS of (3.6) the following is obtained:

$$\int \phi(r_0 Y - y') \hat{\eta}(y') w(y') dy' = g^{(0)}(Y; \hat{\eta}) \phi(0) + \epsilon g^{(1)}(Y; \hat{\eta}) \phi'(0) + \frac{\epsilon^2}{2} g^{(2)}(Y; \hat{\eta}) \phi''(0) + O(\epsilon^3) \quad (\text{A } 2)$$

where the functions $g^{(n)}(y; \hat{\eta})$ are defined by

$$g^{(n)}(Y; \hat{\eta}) = \frac{L_R^n}{(\kappa^2 - 1)^{n/2}} \int |Y - Y'|^n \hat{\eta}(r_0 Y') W(Y') dY', \quad (\text{A } 3)$$

the function $W(Y)$ is defined in (3.2) and the identity $r_0 = \epsilon L_R \sqrt{\kappa^2 - 1}$ is used.

The expansion of (3.6) is then obtained by substituting from (3.11) and (A 2) together with (3.13) and (3.14) and collecting like powers of ϵ . The $O(1)$ terms give

$$(U(0) - c_0) \hat{\eta}_0 = \phi(0) \int \hat{\eta}_0(r_0 Y') W(Y') dY'. \quad (\text{A } 4)$$

Likewise, the $O(\epsilon)$ terms give

$$\left(U'(0) f^{(1)}(Y) - c_1 \right) \hat{\eta}_0 + (U(0) - c_0) \hat{\eta}_1 = \phi'(0) g^{(1)}(Y; \hat{\eta}_0) + \phi(0) \int \hat{\eta}_1(r_0 Y') W(Y') dY', \quad (\text{A } 5)$$

and the $O(\epsilon^2)$ terms give

$$\begin{aligned} & \left(\frac{U''(0)}{2} f^{(2)}(Y) - c_2 \right) \hat{\eta}_0 + \left(U'(0) f^{(1)}(Y) - c_1 \right) \hat{\eta}_1 + (U(0) - c_0) \hat{\eta}_2 \\ &= \frac{\phi''(0)}{2} g^{(2)}(Y; \hat{\eta}_0) + \phi'(0) g^{(1)}(Y; \hat{\eta}_1) + \phi(0) \int \hat{\eta}_2(r_0 Y') W(Y') dY'. \end{aligned} \quad (\text{A } 6)$$

Appendix B. Error estimate for equations (3.26) and (3.27)

Equations (3.26) and (3.27) show the structure and phase speed of the discrete normal mode, with stated as $O(\epsilon^3)$ and $O(\epsilon^4)$ respectively. Here these results are derived in order to justify the error estimates.

The discrete normal mode has the form

$$\hat{\eta}(r_0 Y) = \hat{\eta}_0 + \epsilon^2 \hat{\eta}_2(r_0 Y) + \epsilon^3 \hat{\eta}_3(r_0 Y) + O(\epsilon^4) \quad (\text{B } 1)$$

where $\hat{\eta}_0$ is a constant, $\hat{\eta}_2$ is given by (3.24), and $\hat{\eta}_3$ has not been derived explicitly but similarly to $\hat{\eta}_2$ can be chosen to satisfy $\int \hat{\eta}_3(y) w(y) dy = 0$ by a rescaling of $\hat{\eta}_0$. Substituting into (3.6) gives

$$\hat{\eta}(y) = \hat{\eta}_0 \frac{\phi_s(y)}{U_s(y) - c} + \frac{\epsilon^2}{U_s(y) - c} \int \phi(y - r_0 Y') \hat{\eta}_2(r_0 Y') W(Y') dY' + O(\epsilon^3). \quad (\text{B } 2)$$

At first sight the second term on the RHS is $O(\epsilon^2)$, however $\phi(y - r_0 Y') = \phi(y) + O(\epsilon)$ and $\int \hat{\eta}_2(r_0 Y') W(Y') dY' = 0$ trivially. Therefore (B 2) is equivalent to (3.26). Similarly,

substituting (B 2) into (3.7) gives

$$\hat{\eta}_0 c = \hat{\eta}_0 \int (U_s(y) - \phi_s(y)) w(y) dy + \int (U_s(y) - \phi_s(y)) (\epsilon^2 \hat{\eta}_2(r_0 Y') + \epsilon^3 \hat{\eta}_3(r_0 Y')) W(Y') dY' + O(\epsilon^4) \quad (\text{B 3})$$

and the task here is to show that the second term on the RHS is at least $O(\epsilon^4)$. To this end, it is noted that $U_s(r_0 Y) - \phi_s(r_0 Y) = U(0) - \phi(0) + O(\epsilon^2)$, and as above utilising that $\int \hat{\eta}_2(r_0 Y') W(Y') dY' = \int \hat{\eta}_3(r_0 Y') W(Y') dY' = 0$ gives the result.

Appendix C. Derivation of dispersion relation for the α -turbulence model

Here a derivation is presented of the formulae given in section 4.1 for the α -turbulence family of inversion operators with Green's function (4.8). These are the sharp PV front jet profile (4.9) and dispersion relation (4.10), and the leading-order correction to the dispersion relation for a slightly-smoothed PV front (4.11).

To derive the basic state jet profile (4.9), (4.8) is substituted into (4.2) to give

$$U(y) = -\Delta \Psi(\alpha) \int \left((x^2 + y^2)^{\alpha/2-1} - (x^2 + y_0^2)^{\alpha/2-1} \right) dx. \quad (\text{C 1})$$

This integral is evaluated by first differentiating with respect to y to give

$$U'(y) = -\Delta \Psi(\alpha) (\alpha - 2) y \int (x^2 + y^2)^{\alpha/2-2} dx, \quad (\text{C 2})$$

which converges at large x for all $\alpha < 3$, then utilising the identity (obtained from equations (8.380.3) and (3.384.1), Gradshteyn & Ryzhik (2000))

$$\int (x^2 + y^2)^\lambda dx = y |y|^{2\lambda} \sqrt{\pi} \frac{\Gamma(-(\lambda + 1/2))}{\Gamma(-\lambda)} \quad \text{for } \lambda < -1/2. \quad (\text{C 3})$$

Substituting (C 3) into (C 2) and integrating with respect to y gives, after substituting for $\Psi(\alpha)$ from (4.8) and using standard gamma function identities given for instance in Iwayama & Watanabe (2010),

$$U(y) = -A(\alpha) (|y|^{\alpha-1} - |y_0|^{\alpha-1}) \quad \text{with } A(\alpha) = -\frac{\Delta}{2 \cos(\pi\alpha/2) \Gamma(\alpha)}, \quad (\text{C 4})$$

where y_0 is the same constant of integration as in (C 1). The expression (C 4) reduces trivially to (4.9) when $\alpha \neq 1$ by choosing $U_0 = A(\alpha) |y_0|^{\alpha-1}$. At $\alpha = 1$ the function $A(\alpha)$ is singular, but the combination (C 4) is regular simplifies to $U(y) = -(\Delta/\pi) \log(|y/y_0|)$.

Next, the meridional structure of the perturbation streamfunction for the sharp PV front is derived by substituting (4.8) into (4.3) to give

$$\phi(y; k) = -\Delta \Psi(\alpha) \int \left((x^2 + y^2)^{\alpha/2-1} - 1 \right) \cos(kx) dx. \quad (\text{C 5})$$

As above, this is evaluated by first differentiating with respect to y to give

$$\phi'(y; k) = -\Delta \Psi(\alpha) (\alpha - 2) y \int (x^2 + y^2)^{\alpha/2-2} \cos(kx) dx, \quad (\text{C 6})$$

which converges at large x for all $\alpha < 3$, and then using the identity (equation (8.432.4), Gradshteyn & Ryzhik (2000))

$$\int (x^2 + y^2)^\lambda \cos(kx) dx = \frac{2^{\lambda+3/2} \sqrt{\pi}}{\Gamma(-\lambda)} \frac{K_{-(\lambda+1/2)}(|ky|)}{|ky|^{-(\lambda+1/2)}} \quad \text{for } \lambda < -1/2, \quad (\text{C 7})$$

where $K_\nu(x)$ is the modified Bessel function of the second kind of order ν . Substituting (C7) into (C6) and integrating with respect to y gives, after substituting for $\Psi(\alpha)$ from (4.8), again using standard gamma function identities together with the recurrence relation $\int K_\nu(z)/z^{\nu-1} dz = -K_{\nu-1}(z)/z^{\nu-1}$,

$$\phi(y; k) = -\frac{A(\alpha)}{\Gamma(\beta)|k|^{\alpha-1}} \frac{2K_\beta(|ky|)}{2^\beta|ky|^\beta}, \quad (\text{C8})$$

where $\beta = (1 - \alpha)/2$. The result (C8) is now used to derive both the dispersion relation for waves on a single sharp PV front via (2.10) and also the correction for the smooth front PV dispersion relation via (4.4). The following expansion is used

$$\frac{2K_\nu(z)}{2^\nu z^\nu} = \frac{\Gamma(\nu)}{z^{2\nu}} \left(1 + \frac{z^2}{4(1-\nu)} + O(z^4) \right) + \frac{\Gamma(-\nu)}{2^{2\nu}} \left(1 + \frac{z^2}{4(1+\nu)} + O(z^4) \right). \quad (\text{C9})$$

Combining (C4) and (C8) then gives

$$U(y) - \phi(y; k) \approx A(\alpha)|y_0|^{\alpha-1} - \frac{B(\alpha)}{|k|^{\alpha-1}} + \frac{1}{|k|^{\alpha-1}} \left(\frac{A(\alpha)|ky|^{\alpha+1}}{2(\alpha+1)} - \frac{B(\alpha)|ky|^2}{2(3-\alpha)} \right) \quad (\text{C10})$$

where

$$B(\alpha) = \frac{\Delta}{2\sqrt{\pi}} \frac{\Gamma((\alpha-1)/2)}{\Gamma(\alpha/2)}. \quad (\text{C11})$$

The result (4.10) follows directly from (C10) evaluated at $y \rightarrow 0$ and the result (4.11) follows from (C10) by defining

$$C_1(\alpha) = \frac{A(\alpha)}{2(\alpha+1)} \quad \text{and} \quad C_2(\alpha) = -\frac{B(\alpha)}{2(3-\alpha)}. \quad (\text{C12})$$

REFERENCES

- DE VRIES, H., METHVEN, J., FRAME, T. H. A. & HOSKINS, B. J. 2009 An interpretation of baroclinic initial value problems: Results for simple basic states with nonzero interior PV gradients. *J. Atmos. Sci.* **66**, 864–882.
- ESLER, J. G. 2004 Benjamin–Feir instability of Rossby waves on a jet. *Q. J. Roy. Meteor. Soc.* **130**, 1611–1630.
- FARRELL, B. F. 1982 The initial growth of disturbances in a baroclinic flow. *J. Atmos. Sci.* **39**, 1663–1686.
- GRADSHTEYN, I. S. & RYZHIC, I. M. 2000 *Table of Integrals, Series and Products*, 6th edn. Jeffrey, A. and Zwillinger, D. (eds), AP.
- GRAY, S. L., DUNNING, C. M., METHVEN, J., MASATO, G. & CHAGNON, J. M. 2014 Systematic model forecast error in Rossby wave structure. *Geophys. Res. Lett.* **41**, 2979–2987.
- HARVEY, B. J. & AMBAUM, M. H. P. 2010 Instability of surface temperature filaments in strain and shear. *Q. J. Roy. Meteor. Soc.* **136**, 1506–1513.
- HARVEY, B. J. & AMBAUM, M. H. P. 2011 Perturbed Rankine vortices in surface quasi-geostrophic dynamics. *Geophys. & Astro. Fluid Dyn.* **105**, 377–391.
- HELD, I. M., PIERREHUMBERT, R. T., GARNER, S. T. & SWANSON, K. L. 1995 Surface quasi-geostrophic dynamics. *J. Fluid Mech.* **282**, 1–20.
- IWAYAMA, T. & WATANABE, T. 2010 Greens function for a generalized two-dimensional fluid. *Phys. Rev. E* **82**, 036307.
- JUCKES, M. 1995 Instability of surface and upper-tropospheric shear lines. *J. Atmos. Sci.* **52**, 3247–3262.
- JUCKES, M. 1998a Baroclinic instability of semi-geostrophic fronts with uniform potential vorticity. I: An analytic solution. *Q. J. Roy. Meteor. Soc.* **124**, 2227–2257.
- JUCKES, M. 1998b Baroclinic instability of semi-geostrophic fronts with uniform potential

- vorticity. II: Comparison of analytic and numerical solutions. *Q. J. Roy. Meteor. Soc.* **124**, 2259–2290.
- ORR, W. M'F. 1907 The stability or instability of the steady motions of a perfect liquid and of a viscous liquid. Part I: A perfect liquid pp. 9–68.
- PIERREHUMBERT, R. T., HELD, I. M. & SWANSON, K. L. 1994 Spectra of local and nonlocal two-dimensional turbulence. *Chaos, Solitons and Fractals* **4**, 1111–1116.
- PLOUGONVEN, R. & VANNESTE, J. 2010 Quasigeostrophic dynamics of a finite-thickness tropopause. *J. Atmos. Sci.* **67**, 3149–3163.
- PULLIN, D. I. 1992 Contour dynamics methods. *Ann. Rev. Fluid Mech.* **24**, 89–115.
- RIVEST, C., DAVIS, C. A. & FARRELL, B. F. 1992 Upper-tropospheric synoptic-scale waves. Part I: Maintenance as Eady normal modes. *J. Atmos. Sci.* **49**, 2108–2119.
- SCOTT, R. K., DRITSCHEL, D. G., POLVANI, L. M. & WAUGH, D. W. 2004 Enhancement of Rossby wave breaking by steep potential vorticity gradients in the winter stratosphere. *J. Atmos. Sci.* **61**, 904–918.
- SWANSON, K. L., KUSHNER, P. J. & HELD, I. M. 1997 Dynamics of barotropic storm tracks. *J. Atmos. Sci.* **54**, 791–810.
- VALLIS, G. K. 2006 *Atmospheric and Oceanic Fluid Dynamics*. Cambridge University Press.
- VERKLEY, W. T. M. 1994 Tropopause dynamics and planetary waves. *J. Atmos. Sci.* **51**, 509–529.
- ZABUSKY, N. J., HUGHES, M. H. & ROBERTS, K. V. 1979 Contour dynamics of the Euler equations in two dimensions. *J. Comput. Phys.* **30**, 96–106.
- ZHU, D. & NAKAMURA, N. 2010 On the representation of Rossby waves on the β -plane by a piecewise uniform potential vorticity distribution. *J. Fluid Mech.* **664**, 397–406.